LAWRENCE
LIVERMORE
NATIONAL
LABORATORY

LLNL-CONF-476453

Computational Hydrocode Study of Target Damage due to Fragment-Blast Impact

T. Hatch-Aguilar, F. Najjar, E. Szymanski

March 28, 2011

26th International Symposium of Ballistics
Miami, FL, United States
September 12, 2011 through September 16, 2011

Disclaimer

Conference: 26th International Symposium of Ballistics – Miami, FL September 2011
http://www.ndia.org/meetings/1210/Pages/default.aspx
Session: Terminal Ballistics and Impact Physics
Title: Computational Hydrocode Study of Target Damage due to Fragment-Blast Impact
Authors: Thomas J. Hatch-Aguilar, NAWCWD, China Lake, CA; Fady M. Najjar*, B-Division, LLNL, Livermore, CA; & Edwin W Szymanski, NAWCWD, China Lake, CA.
Classification: UNCLASSIFIED
Distribution Statement: A, Public Release Unlimited Distribution

Introduction:
A target's terminal ballistic effects involving explosively generated fragments, along with the original blast, are of critical importance for many different security and safety related applications. Personnel safety and protective building design are but a few of the practical disciplines that can gain from improved understanding combined loading effects. Traditionally, any engineering level analysis or design effort involving explosions would divide the target damage analysis into two correspondingly critical areas: blast wave and fragment related impact effects. The hypothesis of this paper lies in the supposition that a linear combination of a blast-fragment loading, coupled with an accurate target response description, can lead to a non-linear target damage effect. This non-linear target response could then stand as the basis of defining what a synergistic or combined frag-blast loading might actually look like. The table below, taken from Walters, et. al. [9] categorizes some of the critical parameters driving any combined target damage effect and drives the evaluation of results.

Table 1: Target physical characteristics involved in a generalized impact problem

	Low Velocity Impact	High Velocity Impact
Extent of deformation	Global	Local
Modal Response	Low Frequency	High Frequency
Loading/response time	1ms-1s	Sub-milliseconds
Strains	0.5-10%	>60%
Strain Rates	10^{-2}-10^{1} s^{-1}	>10^{5} s^{-1}
Hydrodynamic Pressure Magnitude	0 (σ_y)	10-100 (σ_y)
Failure Mechanism	Large Plastic Flow	Physical Separation of Material

Source: (9)

Based on the above table it becomes clear that any combined frag-blast analysis would need to account for the target response matching similar ranges for the mechanics described above. Of interest are the critical times upon which a blast event or fragment impact loading occurs relative to the target's modal response.

A blast, for the purposes of this paper is defined as the sudden release of chemical energy from a given material (henceforth referred to as an energetic material) onto its surrounding medium. During the coupling mechanism a discrete or discontinuous shockwave is generated. This shockwave travels outward from the source transferring energy and momentum to any surrounding objects including personnel and engineering structures. From an engineering

perspective blast effects are typically characterized by way of physical characteristics such as Peak Pressure (PP), Time of Arrival (TOA), Pressure-Impulse (PI) and Time of Duration (TD). Other peculiarities include the radial decrease in pressure from the source, any fireball size measurement, and subsequent increase in temperature from the passing of the shockwave through the surrounding medium. In light of all of these metrics, the loading any object receives from a blast event becomes intricately connected to the distance between itself and the source. Because of this, a clear distinction is made between close-in effects and those from a source far away from the object of interest [10].

Explosively generated fragments on the other hand are characterized by means of their localized damage potential. Metrics such as whether the fragment penetrates or perforates a given object is quantified as well as other variables including fragment's residual velocity, % kinetic energy decrease, residual fragment mass and other exit criteria. A fragment launched under such violent conditions could easily be traveling at speeds in excess of 2500 ft/s. Given these speeds it is conceivable to imagine how any given fragment could deliver a concentrated load to a target and penetrates through walls, vehicles or even the protection systems of nearby personnel. This study will focus on the individual fragment-target impact event with the hopes of expanding it to eventually include statistical procedures.

Since this is a modeling excursion into the combined frag-blast target damage effects the numerical methods used to frame this problem become important in-so-far as the simulations are done in a consistent manner. For this study a Finite-Element based Hydrocode solution called ALE3D (ALE=Arbitrary Lagrangian-Eulerian) was utilized. ALE3D is developed by Lawrence Livermore National Laboratory (Livermore, CA), and as this paper will show, successfully implemented a converged ALE formulation including as many of the different aspects needed to query the synergistic damage on a given target. Further information on the modeling setup is included below.

Model Setup and Configurations:

In order to simplify the variability of any system involving both blast and fragment impact and as a preliminary course of action, one component of each was studied. This includes one source for a blast wave and a single fragment impact event. The idea pursued is that once properly designed, these two individual effects would be clearly differentiated in the data collection process. An additional simplification was made by looking at the temporal distribution of the incident events impacting a target: 1) a blast wave impacting a target before the fragment ("bbf"), 2) a combined or coincident impact of both blast and fragment loadings ("cbf") and 3) a fragment target impact before the blast wave ("fbb"). Based on these three devised cases two control configurations must be established: 4) a blast only event against the same target ("b") and 5) a fragment impact event ("f"). The objective is to better understand the underlying physics in an attempt to highlight any synergistic damage effects. All models were implemented by means of a 2D axis-symmetric boundary condition with the fragment, blast and target co-linearly located along the longitudinal axis as seen in Figure 1. This 2D axis-symmetric construct allowed for a significantly faster turn-around in the calculations by exploiting the inherent cylindrical symmetry of the problem. Figure 2 shows 3D "revolved" images of the problem designed for the different case scenarios.

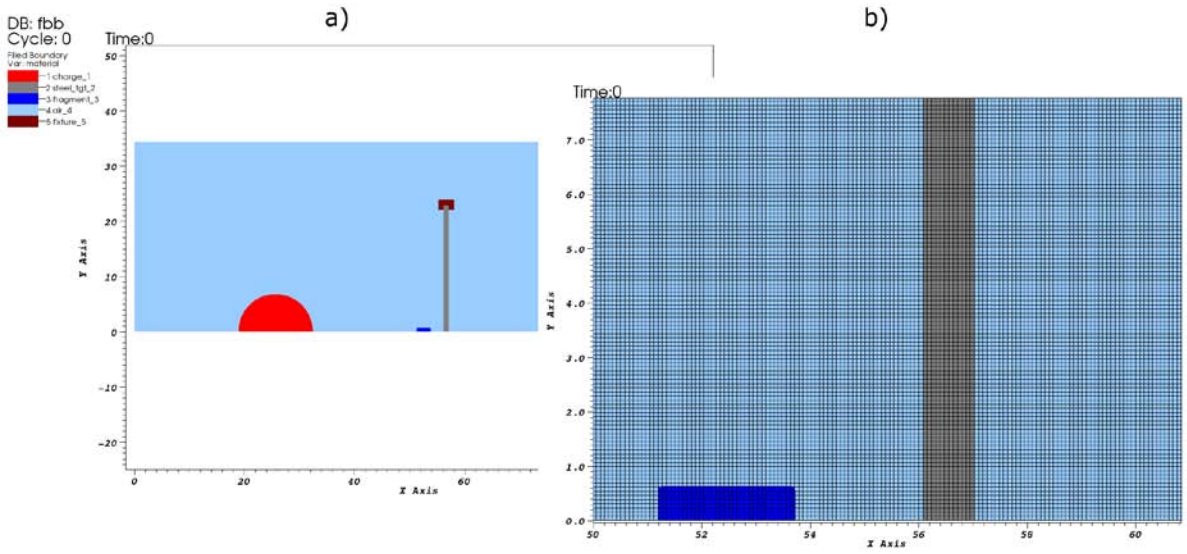

Figure 1: 2D model configurations for the "fbb" steel target case scenario: a) Material plot file highlighting the 2D axis-symmetrical boundary condition, b) Starting mesh description (uniform mesh distribution) focusing on the fragment target area. All length units listed in "cm".

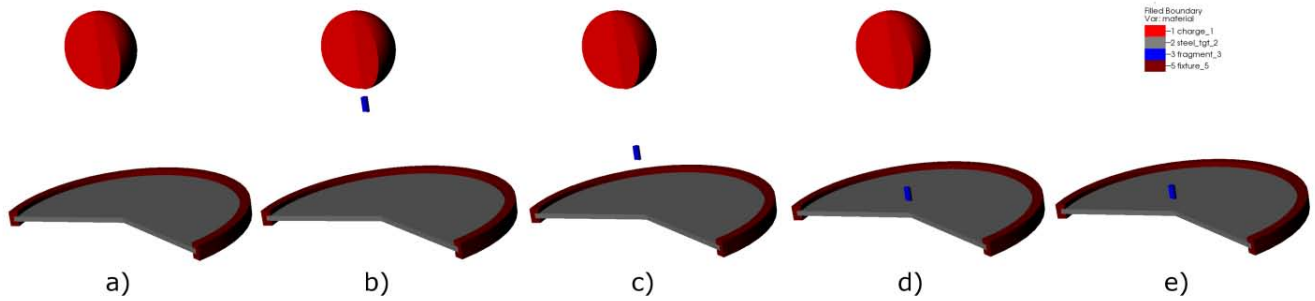

Figure 2: Material plot files (3D) of the different configurations to be studied: a) blast, b) blast before frag, c) combined frag-blast, d) frag before blast, e) frag. Steel target is pictured.

The run matrix utilized to study the synergistic effects of a blast-fragment impact is presented in Table 2.

Table 2: Modeling Run Matrix

Run Matrix	Acronym	Steel	Aluminum	Titanium
blast	b	C	C	C
blast before frag	bbf	X	X	X
combined blast-frag	cbf	X	X	X
frag before blast	fbb	X	X	X
frag	f	C	C	C

C = control, X= combined effects numerical excursions

Blast Details:

A sphere of homogenized High Explosive (HE) was introduced as the sole source for the blast loading. In order to simplify the selection of the explosive an ideal type was chosen (TNT) given

the commonality and conventional nature of the energy release [10]. The HE was assumed to detonate at the center of the sphere with the burn front traversing outward. Numerically this was implemented by using a "programmed burn" model in combination with a Jones-Wilkins-Lee (JWL) Equation of State (EOS) [1, 5-6]. The JWL model relates specific volume of the HE material to the pressure state as seen below:

$$P = A\left(1 - \frac{\omega}{R_1 * v}\right) * e^{-R_1 * v} + B\left(1 - \frac{\omega}{R_2 * v}\right) * e^{-R_2 * v} + \frac{\omega}{v} * e_0$$

where:

P = Pressure
ν = Relative volume
A, B, R_1, R_2, ω, e_0 = JWL coefficients

Tables 3 and 4 show the parameters used to model the energy release from the sphere of TNT.

Table 3: JWL TNT Parameters

A (Mbar)	B (Mbar)	R_1	R_2	ω	e_0 (Mbar)
3.73	3.74	4.15	0.9	0.35	0.060

Sources: (5-6)

Table 4: Additional HE details

	Value	Units
Charge Weight	5	lb
	2.267	kg
Charge Density	1.63	g/cm^3
Charge Radius	6.743	cm
Detonation Speed	0.69	cm/us
Time for total detonation	9.77	us
Stand-off distance to target	1	ft
	30.48	cm
Target surface TOA	~52	us

Sources: (1-4)

Fragment Details:

The fragment used to impact the target was chosen to be representative of an explosively generated type. A simplified version was designed and consisted of a 0.5 inch diameter, L/D=2, right cylinder steel frag. The impact speed was fixed at the initial condition of 6,500 ft/s normal to the surface of the target. Figures 1-2 shows how the fragment was introduced into the

modeling space. It was aligned along the longitudinal axis of the target plate and positioned at three distinct locations based on the desired configuration ("bbf", "cbf" or "fbb"). The exact positioning involved calculating the blast wave TOA from the "blast-only" configuration (estimated at ~52 us) and then introducing a time interval (fixed at 40 us) for the fragment impact time. The time interval was chosen in order to provide sufficient time for each loading event to be discerned from each other in the data collected. Using this method both the "bbf" and the "fbb" layout were devised. For the "cbf" configuration the location of the fragment was made so that both the fragment and blast wave would reach the target surface at the same TOA estimated above. The table below presents the data for the fragment-target offset distances.

Table 5: Fragment-Target Offset Distances

Configuration	Offset Distance (cm)
blast before frag	18.45
combined blast-frag	10.40
frag before blast	2.35
frag only	2.35

The material composition of the fragment was surrogated with that of an AISI 1020 hot rolled steel alloy configuration. This seemed appropriate for a preliminary study further research into a more suitable surrogate is left for future work. Table 6 highlights the material properties used modeling the fragment.

Table 6: Fragment Material Properties

Property	Value	Units
Density	7.87	g/cm^3
Young's Modulus	2.05	Mbar
Poisson's Ratio	0.29	
Initial Yield Strength	2.05	kbar
Tangent Modulus	1.05	Mbar
Effective Plastic Strain to Failure	25%	

Sources: (1-4)

Target Details:
In order to capture the possible synergistic damage of a combined frag-blast impact event a 3ft (91.44 cm) circular plate target composed of either mild steel, titanium or aluminum was placed 1 foot (30.48 cm) away from the HE source. The target was held in place by a hardened steel "c-clamp" type fixture around the periphery of the circular plate. The plate was 0.375 inches

(0.9525 cm) thick for a T/D (target thickness / fragment diameter) ratio of 0.75. Table 7 provides more details regarding the mechanical properties of each target material explored.

Table 7: Target Material Properties

	Aluminum	Steel	Titanium	
Surrogate Alloy	2024-T6	Mild Steel ~AISI 1000	Ti-6Al-4V	
Density	2.78	7.84	4.43	g/cm^3
Young's Modulus	0.724	2.000	1.140	Mbar
Poisson's Ratio	0.33	0.29	0.33	
Initial Yield Strength	3.45	1.65	8.30	kbar
Tangent Modulus	0.362	1.000	0.570	Mbar
Effective Plastic Strain to Failure	5%	9%	10%	
Areal Density	2.67	7.43	4.22	g/cm^2

Sources: (1-4)

Material Response Models

From a materials perspective an engineering level model was implemented for the target, fixture and fragment geometries, all based on a distinctive bi-linear yield curve response. This material response is dominated by the constitutive behavior and the equation of state calculation disregarding thermal influence [8]. It produces an elastic-plastic response of the form (constitutive form):

$$\sigma = \sigma_o + E_p \varepsilon$$

$$E_P = \frac{E_T E}{E - E_T}$$

Where

$E_P =$ Plastic hardening modulus
$\sigma_0 =$ Initial yield Strength
$E =$ Young's modulus
$\varepsilon =$ Effective plastic strain
$E_T =$ Tangent modulus

For the EOS the following relationship was implemented:

$$P = K * \mu$$

$$\mu = \left(\frac{1}{v}\right) - 1$$

Where

ν = Relative volume
K = Bulk modulus

Numerical Methodology:
Before any of the "run matrix" scenarios were executed, a mesh resolution analysis was performed in an attempt to maximize solution convergence. The following table exemplifies the iterations observed. The original mesh created constituted what would be the first row in Table 8. Figure 3 shows two key measure of goodness evaluated for convergence: total momentum transferred to the target plate and total kinetic energy absorbed by the target. For each metric a convergence can be observed as the mesh is refined. A 5% relative error criterion was established for our evaluation purposes. It was found that any mesh resolution multiplier greater than 2.5 would satisfy the requirement from a target momentum perspective. However from a target kinetic energy evaluation the relative % error criterion points to a mesh resolution multiplier greater than 3.5 for the same scenario. Given the total quantity of simulations to run (15 in total), and the data processing that goes along with such an endeavor, minimizing the total wall-time became the deciding factor among both momentum and kinetic energy mesh resolution recommendations. A mesh resolution multiplier of 2.5 was chosen for the production type calculations based on the run-matrix presented previously. Running one such production calculation (total model time = 250 us), a combined blast-frag steel target simulation took approximately 6,771 seconds (~1.8 hours) on 72 processors. Because of the practicality of such a procedure, this became the accepted mesh density for all of the calculations in the run matrix.

Table 8: Mesh Resolution Multiplier and associated mesh metrics

Mesh Resolution Multiplier	Total # of elements (10^3 elements)	# elements across target thickness	# elements across fragment radius	Mesh Size (cm / element)
1.0	87	5	3	1.91
1.5	197	8	5	1.27
2.0	350	10	7	0.95
2.5	547	13	8	0.76
3.0	547	15	10	0.64
3.5	1,096	18	12	0.54
4.0	1,431	20	13	0.48

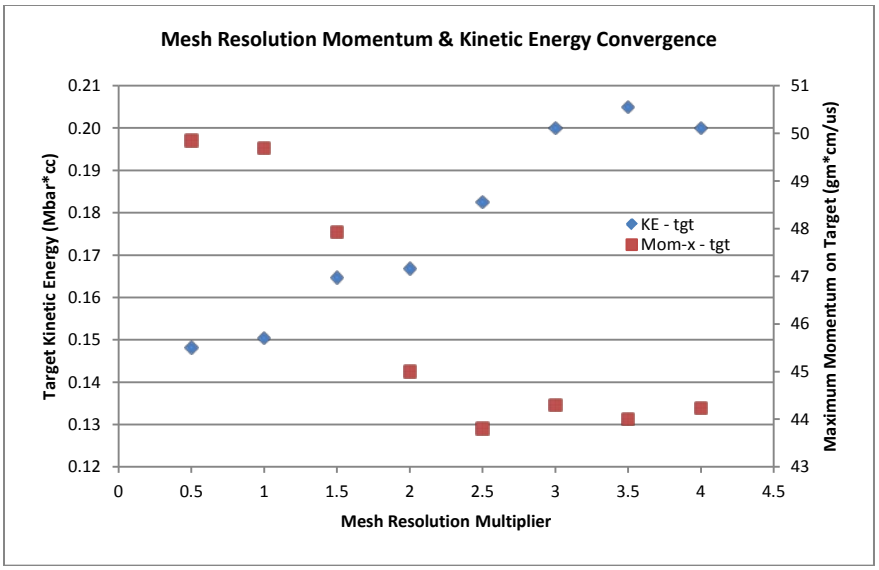

Figure 3: Mesh Resolution Convergence Study

Results and Analysis:

For all of the configurations evaluated the fragment was able to perforate the corresponding target. Because of this, the fragment's residual speed became a good initial metric for comparing the relative momentum transfer to the target. Figure 4 plots the fragment's residual speed after perforating their respective target normalized by the incident speed. Lower values indicate a higher energy loss for the fragment and inherently an increased momentum transfer to the target. For Aluminum and Titanium targets this difference is not as pronounced between the configurations as with the Mild Steel target. All of these curves hint at a preferential transfer of energy or momentum for the "bbf" configuration. The authors note how the normalized residual speed varies in magnitude as a function of the target material's composition, more precisely how it is following the density of the target material involved in the impact. Further examination of this effect is discussed later in this section.

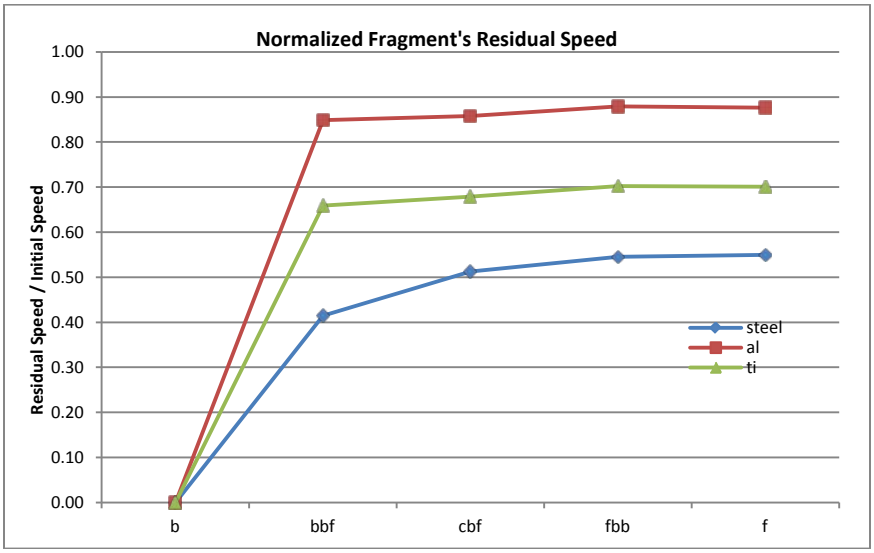

Figure 4: Normalized Fragment's Residual Speed

Looking at the target's absorbed momentum; Figure 5 shows the great disparity between the impulse transferred to the plate from a blast, a frag or combination of frag-blast configurations. The difference between a blast related impulse on target and that available from the single frag devised almost reaches an order of magnitude. This is not entirely surprising as both impulses act over different presented areas, time scales and one provides a more localized (fragment) coupling that the other (blast). However if the transferred impulse on target is normalized by the configuration dependent available incident impulse, a "target impulse transfer efficiency" can be quantified. Figure 6 presents this data highlighting the relative difference between blast and frag impulse transfer efficiencies. Although the "blast" component to the combined effects provides almost an order of magnitude greater momentum compared to the "frag" element, the transfer efficiency is quite low ~18%. Alternatively, the transfer of momentum from a fragment impact is quite limited in comparison with a blast, however the efficiency upon which it can couple to the target can reach values as high as ~80%. The data also shows a similar dependency of the momentum transfer efficiency to the target material composition with higher density targets having increased coupling or efficiencies. The rationale for such a trend lies in the types of shock pressures generated at the time of impact. An estimate of this shock pressure (Ps) compared to the corresponding target strength (St) shows that density effects should dominate all impact configurations involving the fragment and targets devised for this study. Furthermore the Ps/St estimate makes a case for an increased sensitivity favoring the Mild Steel compared to either the Aluminum or Titanium targets by almost an order of magnitude. Since the analysis currently is focusing on the fundamental physics later in the section comparisons are made with regards to actual target response.

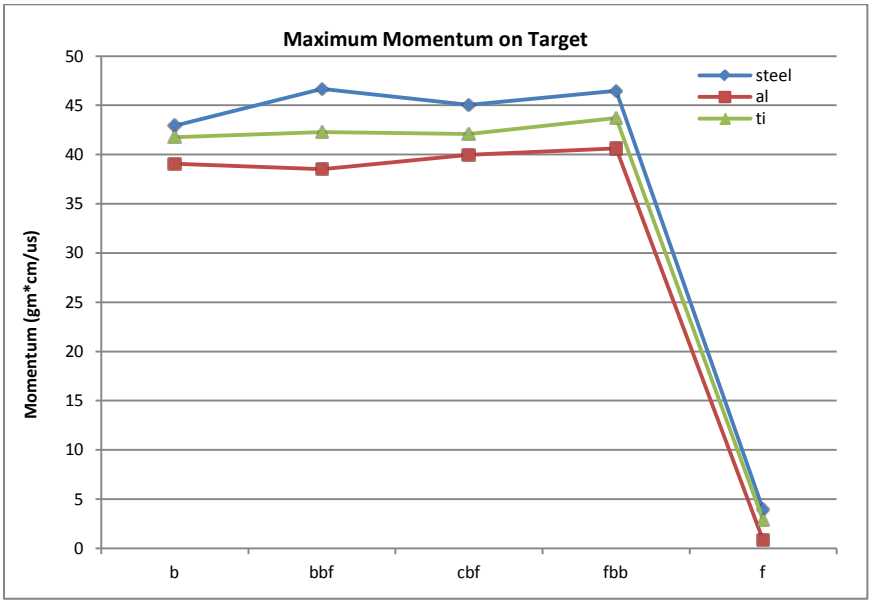

Figure 5: Maximum Momentum on Target

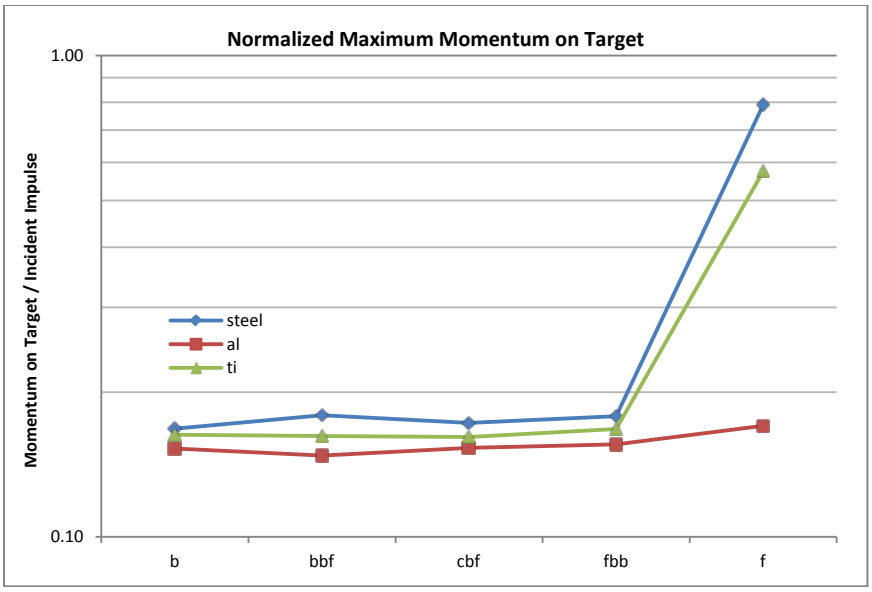

Figure 6: Target Momentum/Impulse Transfer Efficiency

In terms of the kinetic energy on target, Figure 7 shows how any of the combined effects configurations maximizes the energy transfer to the target above any of the individual component (blast or frag). This behavior is seen across the different target material types, although the order of which the maximization occurs is opposite from that observed from the momentum plots. A possible way to understand this discrepancy lies in the difference between momentum and kinetic energy from an order of magnitude perspective. Kinetic energy has a second order velocity term versus the linear term found in the momentum. The interaction of these construct help explain the opposite trend observed herein. The magnitudes of the total target kinetic energy observed normalized by the incident fragment kinetic energy in Figure 8. Titanium and steel targets maximize the amount of kinetic energy absorbed in the "fbb" configuration while the aluminum target prefers to maximize the transfer for the "cbf". Also of interest is how the differences in the kinetic energy between blast and frag effects are not as severe as those observed in the momentum plots indicating improved matching. The steel target minimizes the differences between effects and is something to be explored in subsequent studies.

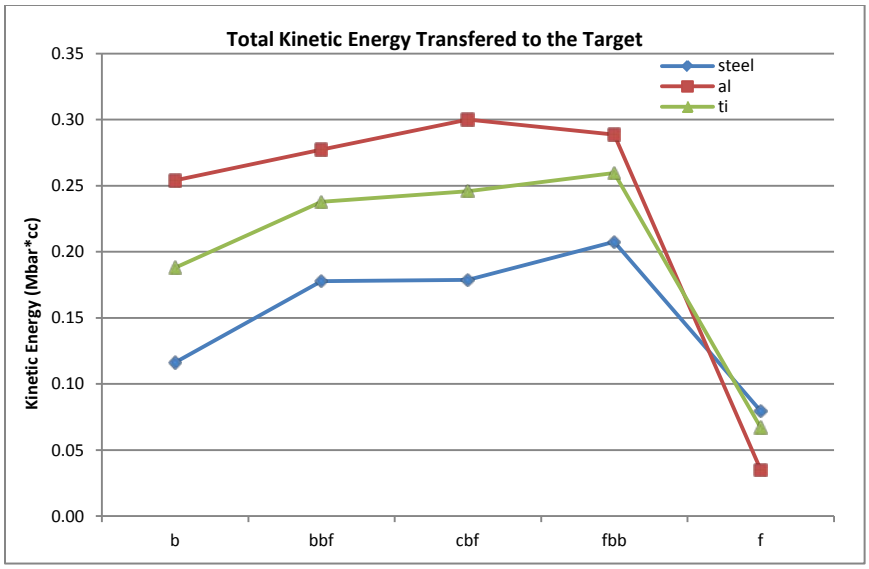

Figure 7: Total Target Kinetic Energy

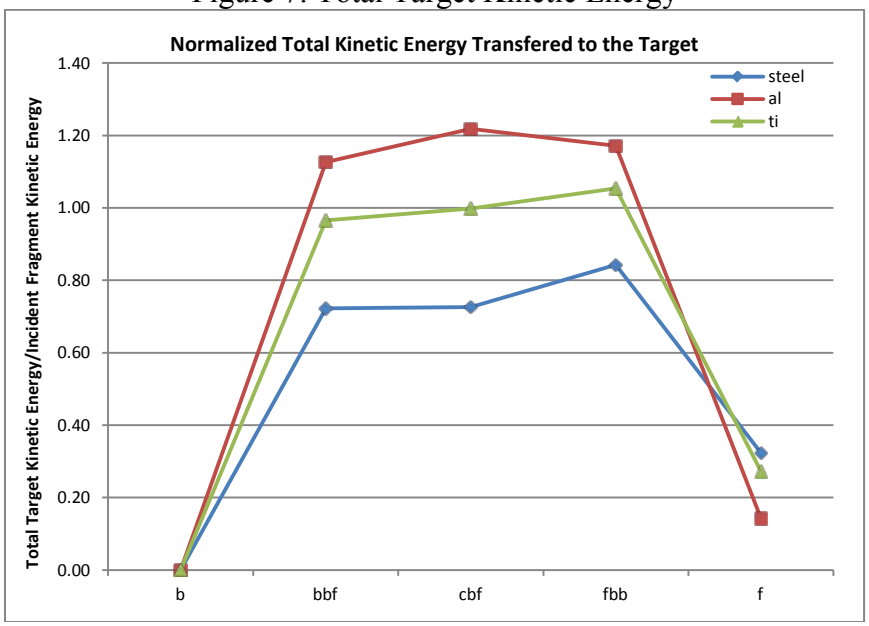

Figure 8: Normalized Total Target Kinetic Energy

If instead of looking at fundamental variables of the system (momentum or kinetic energy) we focus the analysis onto actual damage done to the plate two metrics clearly come to our attention: deflection of the plate and perforated cavity size. Figure 9 shows how the perforated bore size is maximized on the average for any of the combined blast-frag configurations ("bbf", "cbf" or "fbb"). Figure 10 plots the normalized target deflection as a function of the different case scenarios calculated and confirms the trends mentioned previously regarding target density effects in the penetration dynamics. In this case minimizing target density increases target deflection significantly. Opposite to this result maximizing target density increases the average perforated bore size up to 47% more compared to your original fragment diameter.

Given that the theme of this study is exploratory in nature; further examination must be made regarding the bore size and target deflection identification. Currently this is made by measuring

the inner-most radius (for the case of the bore size measurement) along the target thickness however this simplified metric does not account for the complex penetration mechanics observed. At the same time the total time of the simulation was capped at 250 us which may not completely account for the deformed state and it's inherently time dependent behavior. Further studies would have to account for these intricacies and is left for future endeavors.

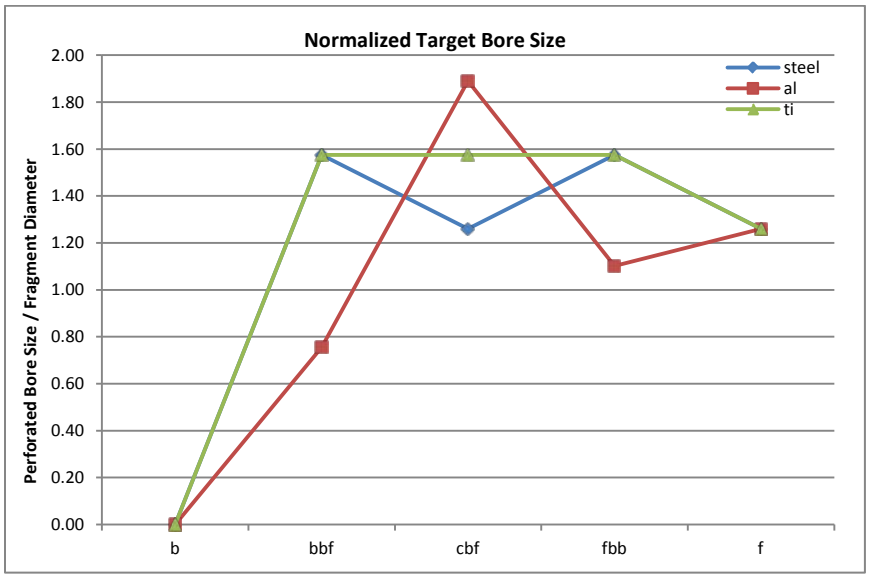

Figure 9: Normalized Target Bore Size at 250 us

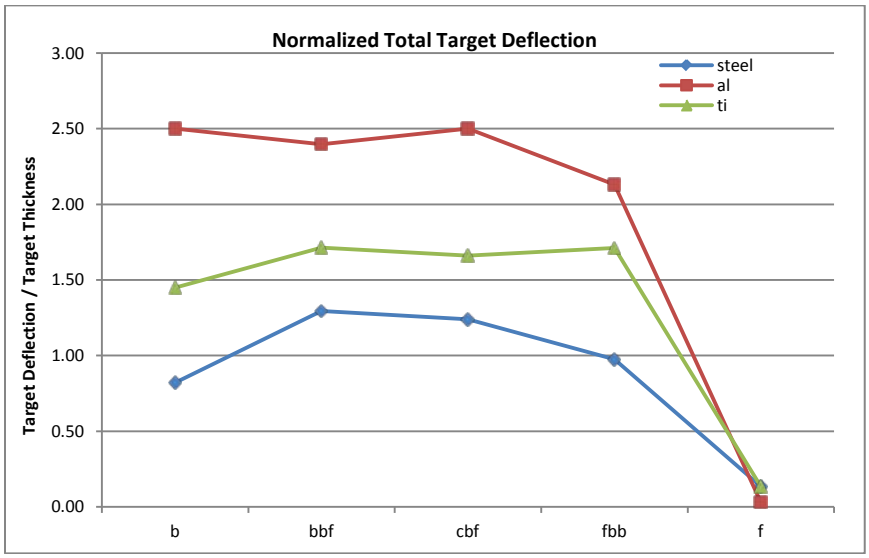

Figure 10: Normalized Total Target Deflection at 250 us

Another comparison is shown in Figure 11 by plotting the target's effective plastic strains at the end of each of the simulations. This visual matrix highlights the spatial distribution of the plastic strain which would be related to observable target damage. As a general statement higher density target materials increase both the severity and spatial distribution of the plastic strains. This follows the trends observed from examining the momentum transfer to the target and not those related to the kinetic energy on target. An exception can be made to this statement based

on the Aluminum target data under the "fbb" configuration which would require further study. Material models and the description utilized throughout this numerical exercise ultimately define the behaviors observed in the output hence further refinement must be taken into account in order to capture any other dynamics not necessarily concerned with density effects. It is left as a follow-on work how these are eventually incorporated into a similarly designed run matrix.

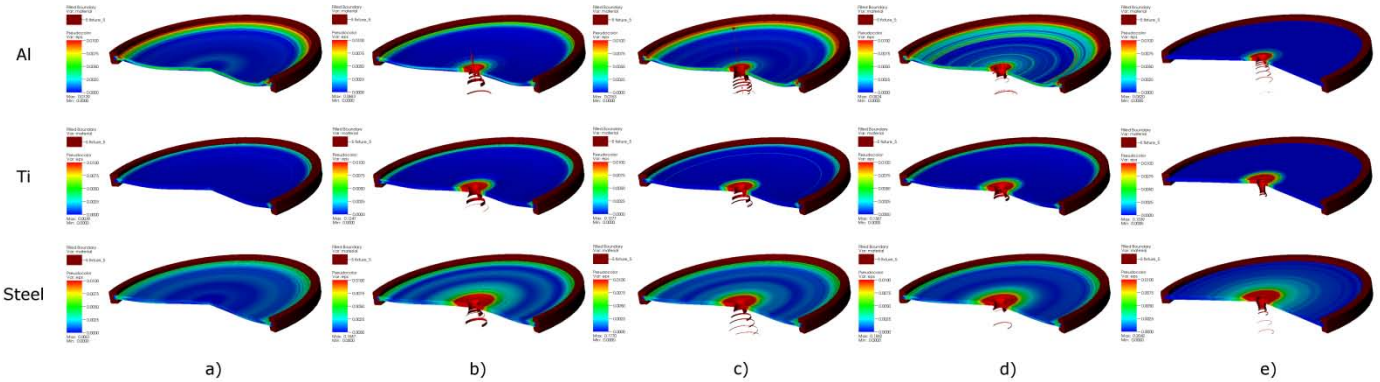

Figure 11: 3D target damage at 250 us (effective plastic strain contour plot)

Conclusions:

This study successfully examined the combined loading from a fragment-blast impact against a notional 0.375 inch thick statically clamped 3 ft in diameter circular plate target. The data sheds light onto the synergistic target damage observed by the sudden release of energy from a 5 lb TNT charge and a 0.5 inch L/D=2 steel fragment traveling at 6500 ft/s. Three different target materials were explored in this paper: an aluminum, titanium and steel alloy compositions while holding constant the blast source and the offset distance in between target and charge. A temporal distribution of the target impact events was studied including a blast-before-fragment, combined-fragment-blast and a fragment-before-blast configuration while holding fixed the time interval between events at 40 us.

The numerical simulations were executed using Lawrence Livermore National Laboratory's ALE3D finite element based hydrocode. A mesh resolution analysis was successfully completed showing how a mesh size of at the most ~0.76 cm/element was able to converge in terms of momentum and kinetic energy on target. Given this, a run matrix totaling 15 simulations was performed with a 250 us total model time for each.

The resulting data was analyzed in terms of a few metrics: maximum momentum on target, total kinetic energy on target, target plate deflection, perforated target bore size and effective plastic strain. The results indicate how density effects (for these particular configurations) play a dominant role in determining the overall target damage. **This is truly a function of the generated shock pressures from the currently devised impact conditions and should be further examined in terms of a range of impact conditions to ascertain validity.** For the current setup the data shows how an increase in the target density maximizes the residual velocity drop for the fragment, preferentially choosing a "bbf" configuration among the different combined frag-blast scenarios. The data also presents the wide disparity in the momentum transferred to the target from either blast or fragment loadings raising the question regarding how

the target would respond against effects of similar magnitudes. This part would have to be explored in subsequent studies. Additionally the momentum transfer from a blast source overshadows the magnitude delivered from the incident fragment impact by almost an order of magnitude while the efficiency of the latter increases to ~80% compared to ~18% for a blast event. An observation is further made into how the increase in target densities increases the momentum absorption. A correlation can be made between the previous statement and the fact that the bore size of the perforated cavity increases along with a target density change, up to a 47% increase in size compared to the original fragment diameter. Another interesting detail lies in how the amount of accumulated plastic strain, along with the respective spatial distribution, follows the increase in target density. The only metric that does not follow the previous tendencies is the maximum target deflection, behaving opposite to the target density change. For all of the materials investigated the data shows that as you increase target density the deflection observed is minimized. The fact that this contradicts the previous direct relationships between target density and both target bore size and plastic strain level only heightens the influence blast has on any combined blast-frag loading. Target plate deflection is more associated with blast effects than fragment impact events given the increased available area of interaction. The coupling that takes place with a blast wave allows for increased transfer of kinetic energy onto the target which translates into a time dependent distributed load-deflection mechanism. By looking at this increased kinetic energy deposition a preferential configuration based on any of the combined frag-blast configurations can be observed. This follows matching behavior for the plate deflection for the steel target set and provides proof of the previous relationships observed. The data from these simulations also shows that as you decrease the target density you increase the plate sensitivity towards blast effects and hence maximize plate deflection. This paper concludes by stating that combined or synergistic target damage is observed as a non-linear response to however linear inputs in terms of the fundamental physics explored such as the kinetic energy on target and maximum momentum on target. More studies are needed to expand the trade space regarding the impact conditions desired to yield such occurrences and is left for future endeavors.

Acknowledgements:
The authors would like to acknowledge the help, guidance and support from the following organizations and individuals: Naval Air Warfare Center – Weapons Division - Mr. Robert Koontz, Mr. Robert Cox, Mr. Gill Cornel, Mr. Barry Ells, Mr. Seth Baynar, Dr. Ying-Ming Lee, United States Department of the Defense – High Performance Computer Modernization Office and the United States Army – Engineering Research and Development Center for exceptional computational resources.

References:

1. ASM Specialty Handbook - Carbon and Alloy Steels, edited by J.R. Davis, Davis & Associates, ASM International, Metals Park, OH, (1996).
2. Engineering Properties of Steels, Philip D. Harvey, editor, American Society for Metals, Metals Park, OH, (1982).
3. Metals Handbook, Vol.1 - Properties and Selection: Irons, Steels, and High-Performance Alloys, ASM International 10th Ed. 1990
4. Metals Handbook, Howard E. Boyer and Timothy L. Gall, Eds., American Society for Metals, Materials Park, OH, 1985.

5. M. Z. Vulitsky, Z. H. Karni, Ship structures subject to high explosive detonation. 7th International LS-Dyna User's Conference. Volume 6 pp 27-34
6. N. Birnbaum, J. Tancreto, K. Hager, Calculations of Blast Loading in the High Performance Magazine with AUTODYN-3D. Report Date: 1994 DTIC - AD Number: ADA507383
7. User's Manual for ALE3D – Volume 1 Lawrence Livermore National Laboratory June 2010 LLNL-SM-433954 Official Use Only / Export Controlled
8. User's Manual for ALE3D – Volume 2 Lawrence Livermore National Laboratory June 2010 LLNL-SM-433954 Official Use Only / Export Controlled
9. Fundamentals of Shaped Charges W.P. Walters / J.A. Zukas. CMC Press. 1989
10. Explosive Loading of Engineering Structures P.S. Bulson. Taylor and Francis Group. 1997

This work performed under the auspices of the U.S. Department of Energy by Lawrence Livermore National Laboratory under Contract DE-AC52-07NA27344.